Supplementary Information *for*

Dielectric permittivity tensor dynamics of in-plane hyperbolic van der Waals $MoOCl_2$ and emergent chiral photonic applications

A. V. Margaryan[1,+], M. L. Sargsyan[1,+], M. H. Hayrapetyan[1], D. A. Karakhanyan[1], K. S. Novoselov[2, 3] & D. A. Ghazaryan[1,]*

[1]Laboratory of Advanced Functional Materials, Yerevan State University, Yerevan 0025, Republic of Armenia

[2]Institute for Functional Intelligent Materials, National University of Singapore, Singapore, 117575, Republic of Singapore

[3]Materials Science and Engineering, National University of Singapore, Singapore, 117575, Republic of Singapore

The correspondence should be addressed to: davitghazaryan@ysu.am

Supplementary Note 1: Cross-polarization angle-resolved Raman spectroscopy of vdW $MoOCl_2$

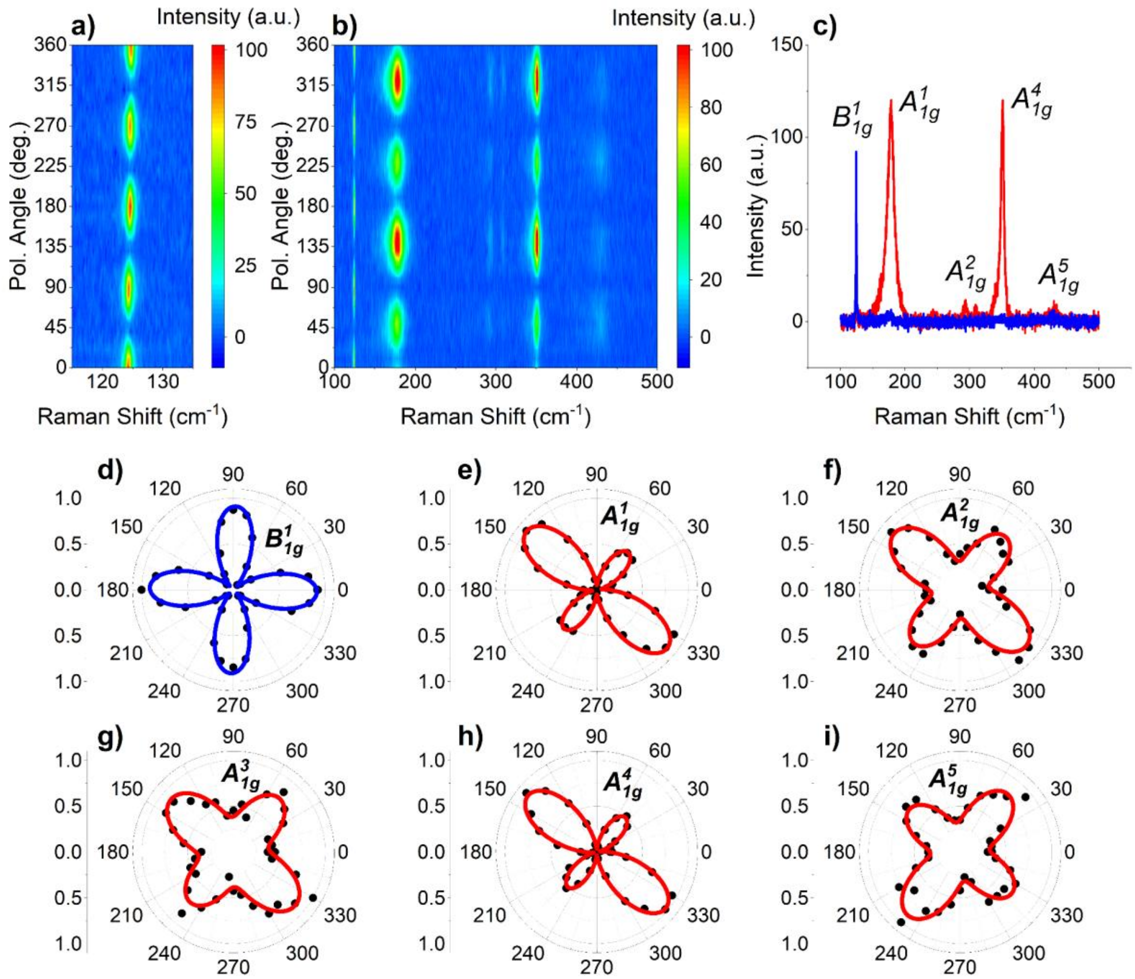

Fig. S1| Cross-polarization Raman mapping of metal-to-insulator in-plane axes of vdW $MoOCl_2$. **a)** and **b)** Angle-resolved Raman intensity map acquired in the co-polarized ($e_i \perp e_i$) configuration for showing the angular evolution of B_g mode at 115-135 cm^{-1} spectral region and (a) the full spectral region of 100-500 cm^{-1} (b). **c)** Raman spectra plots acquired along in-plane dielectric *y*-axis (red curve) and metallic *x*-axis (blue curve). **d-i)** Polar diagrams of the representative A_g and B_g Raman modes shown as a function of the polarization angle ϑ.

For the cross-polarized configuration measurements in backscattering regime, we model the polarization unit vectors as $e_i(\theta) = (cos\theta, sin\theta, 0)$ and $e_s^{||}(\theta) = e_i(\theta)$, $e_s^{\perp}(\theta) = (-sin\theta, cos\theta, 0)$. The substitution of these polarization unit vectors into $J \propto |e_s^T \alpha(j) e_i|^2$ yields the following angular dependencies of $J_{\times}^{A_g} \propto a^2\left[\left(\frac{b}{a} - cos\varphi_{ba}\right)^2 + sin^2\varphi_{ba}\right]sin^2\theta cos^2\theta$ for A_g modes and $J_{\times}^{B_g} \propto (ecos2\theta)^2$ for B_g mode. In addition, for the achievement of a good fit, we also consider that the laser propagation direction was slightly tilted relative to the *z*-axis of vdW $MoOCl_2$ by a small angle ϕ introducing an out-of-plane electric field component (in the case of the cross-polarization measurements configuration). The latter is characterized by η = sinϕ, while the in-plane polarization amplitude is given by $s_0 = \sqrt{1-\eta^2}$. Taking this small deviation into account, the Raman amplitudes in can be expressed as $A_{\times}^{A_g} = c\eta^2 + \frac{{s_0}^2}{2}(b - a)sin\,2\theta + d\eta s_0[cos\theta + sin\theta]$ and $A_{\times}^{B_g} = e{s_0}^2 cos\,2\theta + f\eta s_0[cos\theta - sin\theta]$. Notably, the additional

$c\eta^2$ term in $A_{\times}^{A_g}$ breaks the four-fold symmetry producing unequal lobe intensities observed experimentally for all A_g modes. Interestingly, in cross-polarization configuration, all the detected modes exhibit four-lobed angular patterns. In particular, B_g mode displays maximums at 0°, 90°, 180° and 270° degrees corresponding to the orthogonal condition of the scattered and incident polarizations

Supplementary Note 2: Conventional micro-ellipsometry (an extended dataset)

Additional spectroscopic micro-ellipsometry data obtained by aligning the sample to extract Ψ and Δ along x and y, are shown below. The results exhibit strong direction-dependent variations, clearly revealing the pronounced in-plane optical anisotropy of vdW $MoOCl_2$.

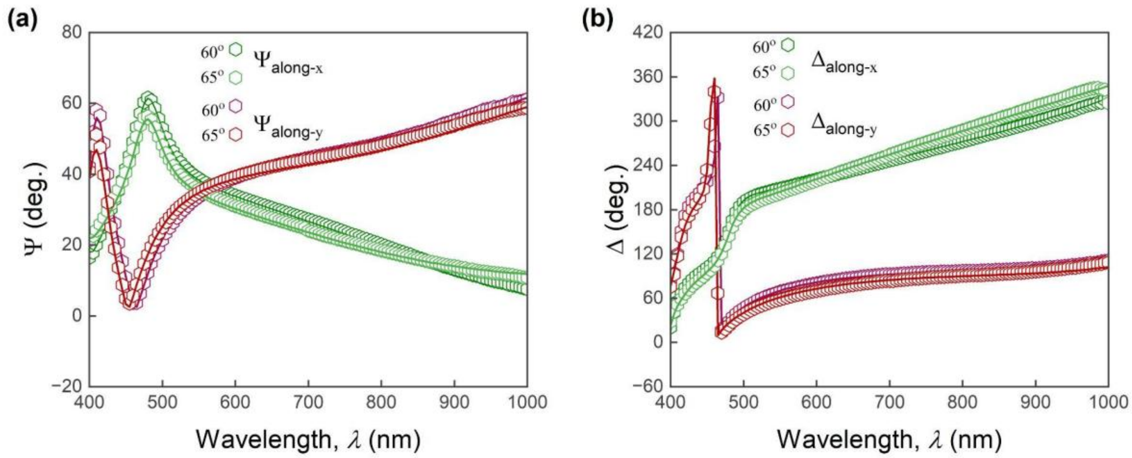

Fig. S2|**a)** Ellipsometric parameter Ψ acquired along the metallic x and dielectric y in-plane axes. **b)** Same as (a), but for the ellipsometric parameter Δ, measured for a 67 nm-thick vdW $MoOCl_2$ sample on a 90 nm Si/SiO_2 substrate at angles of incidence of 60°, 65°.

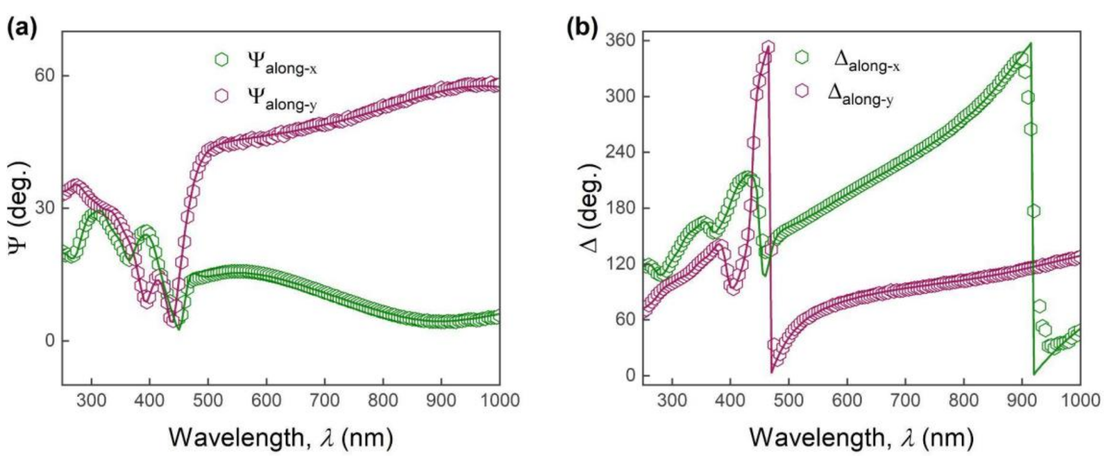

Fig. S3|**a)** Ellipsometric parameter Ψ acquired at an AOI of 65° along the metallic x and dielectric y in-plane axes. **b)** Same as (a), but for the ellipsometric parameter Δ, measured for a 121 nm-thick vdW $MoOCl_2$ sample on a Si substrate.

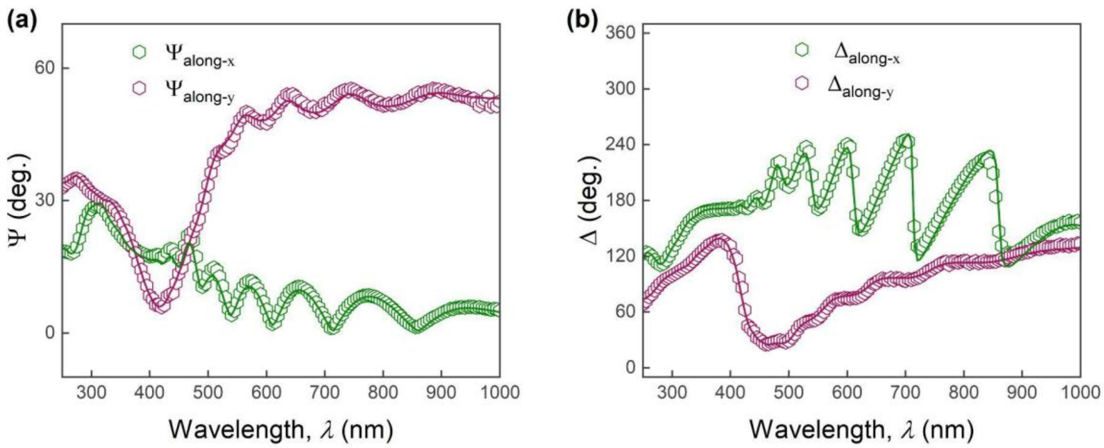

Fig. S4| **a)** Ellipsometric parameter *Ψ* acquired at an AOI of 65° along the metallic *x* and dielectric *y* in-plane axes. **b)** Same as (a), but for the ellipsometric parameter *Δ*, measured for a 720 nm-thick vdW $MoOCl_2$ sample on a Si substrate.

Supplementary Note 3: Muller Matrix micro-ellipsometry dataset

Below are shown the MM measurements in different configurations and the corresponding fits for different vdW $MoOCl_2$ samples.

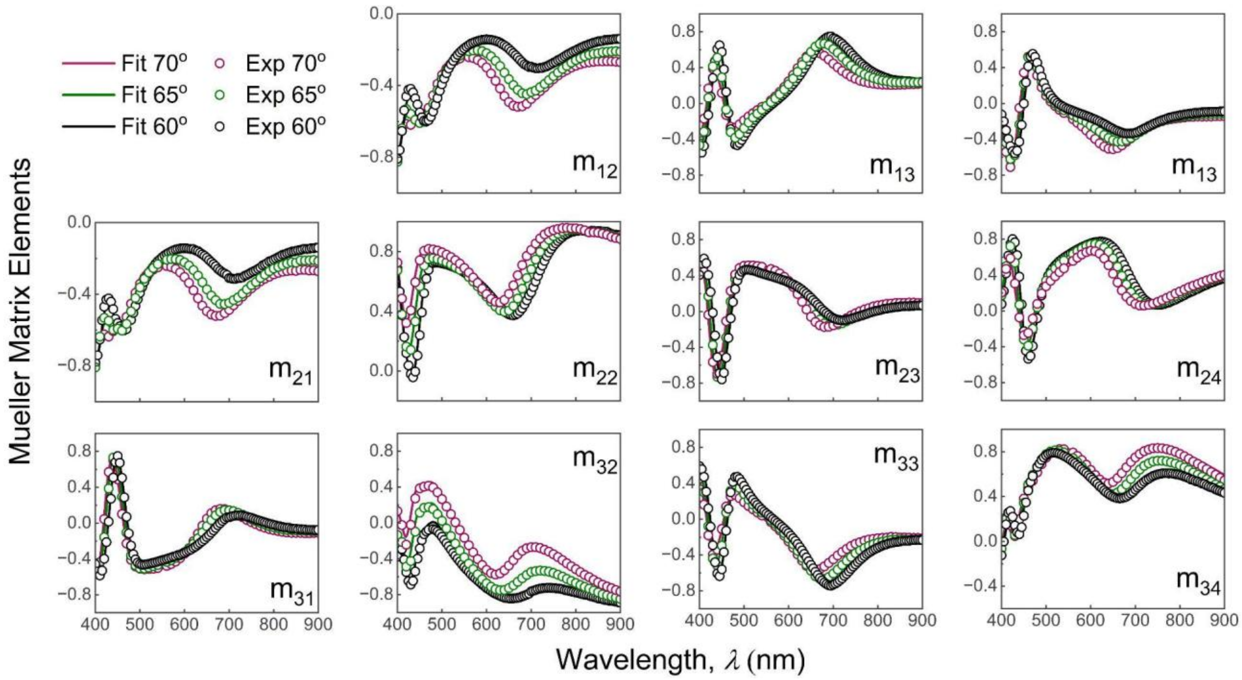

Fig. S5| Mueller matrix elements for a 78 nm-thick vdW $MoOCl_2$ sample on a 295 nm SiO_2/Si substrate at angles of incidence of 60°, 65°, and 70°.

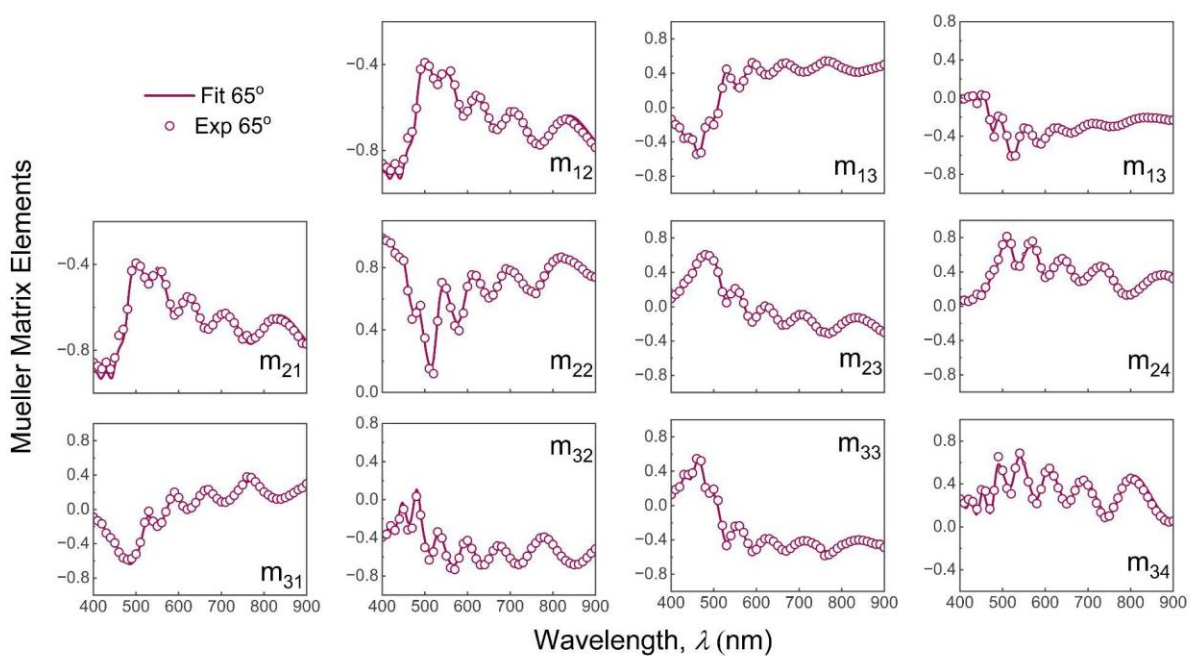

Fig. S6| Mueller matrix elements for a 650 nm-thick vdW $MoOCl_2$ sample on a 295 nm SiO_2/Si substrate.

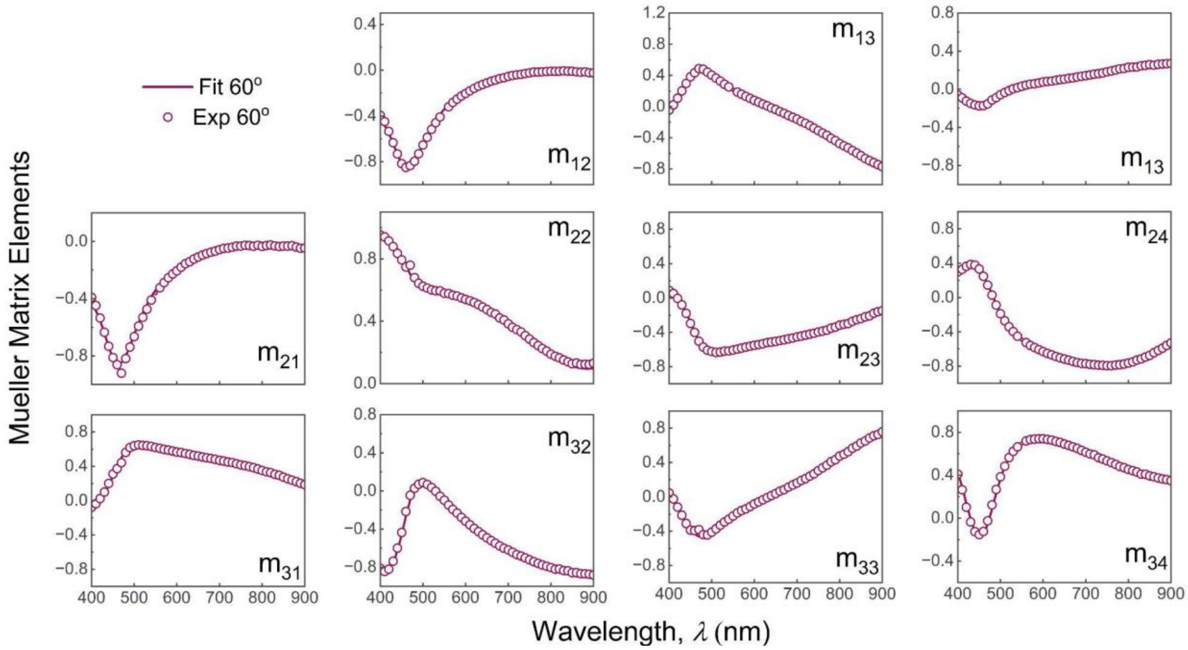

Fig. S7|Mueller matrix elements for a 50 nm-thick vdW $MoOCl_2$ sample on a 90 nm SiO_2/Si substrate.

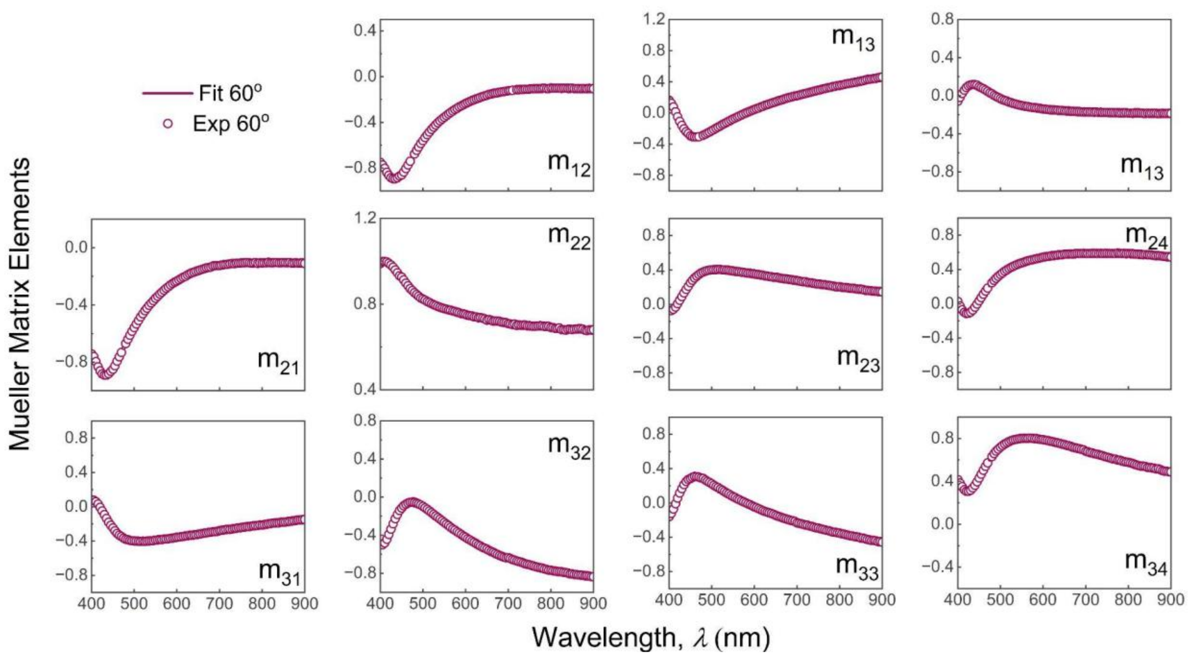

Fig. S8| Mueller matrix elements for a 58 nm-thick vdW $MoOCl_2$ sample on a glass substrate.

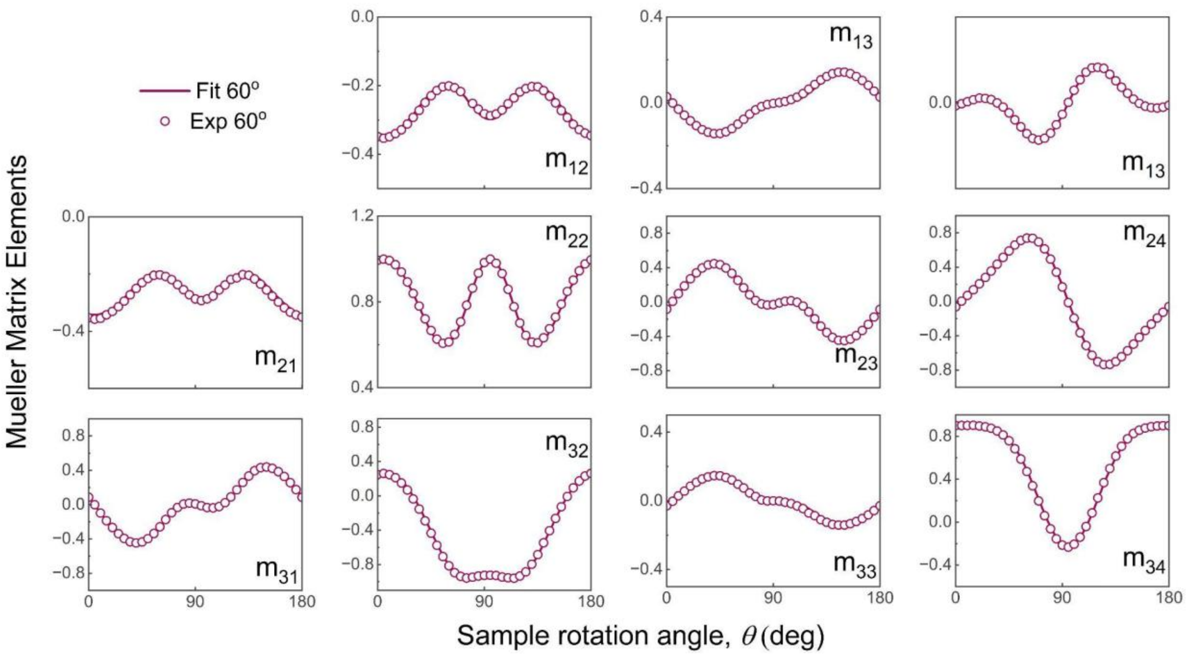

Fig. S9| Mueller matrix elements of a 78 nm-thick vdW $MoOCl_2$ sample on a 295 nm SiO_2/Si substrate, plotted as a function of sample rotation angle.

Supplementary Note 4: The tabulated dielectric permittivity tensor principal components and anisotropic optical constants of vdW $MoOCl_2$

Table S1**.** Tabulated dielectric constants of vdW $MoOCl_2$.

λ (nm)	Re[ε_{zz}]	Im[ε_{zz}]	Re[ε_{xx}]	Im[ε_{xx}]	Re[ε_{yy}]	Im[ε_{yy}]
250.00	4.64	0.00	-0.23	1.97	2.29	4.16
253.75	4.61	0.00	-0.30	2.06	2.48	4.33
257.50	4.58	0.00	-0.38	2.15	2.66	4.35
261.25	4.55	0.00	-0.46	2.25	2.74	4.26
265.00	4.52	0.00	-0.55	2.35	2.71	4.12
268.75	4.50	0.00	-0.64	2.47	2.55	4.00
272.50	4.47	0.00	-0.73	2.59	2.28	3.93
276.25	4.45	0.00	-0.82	2.73	1.92	3.94
280.00	4.43	0.00	-0.92	2.88	1.50	4.08
283.75	4.41	0.00	-1.02	3.04	1.04	4.34
287.50	4.39	0.00	-1.11	3.23	0.57	4.77
291.25	4.37	0.00	-1.20	3.44	0.15	5.37
295.00	4.35	0.00	-1.29	3.67	-0.17	6.14
298.75	4.33	0.00	-1.36	3.92	-0.32	7.06
302.50	4.32	0.00	-1.41	4.20	-0.29	8.05
306.25	4.30	0.00	-1.43	4.50	-0.08	9.08
310.00	4.28	0.00	-1.43	4.82	0.25	10.16
313.75	4.27	0.00	-1.40	5.14	0.78	11.41
317.50	4.26	0.00	-1.34	5.48	1.77	12.83
321.25	4.24	0.00	-1.27	5.82	3.50	14.06
325.00	4.23	0.00	-1.19	6.20	5.78	14.53
328.75	4.21	0.00	-1.09	6.64	7.94	14.04
332.50	4.20	0.00	-0.91	7.15	9.52	13.04
336.25	4.19	0.00	-0.60	7.73	10.59	11.99
340.00	4.18	0.00	-0.08	8.32	11.45	11.01
343.75	4.17	0.00	0.65	8.80	12.20	9.99
347.50	4.16	0.00	1.52	9.07	12.77	8.84
351.25	4.14	0.00	2.41	9.10	13.06	7.64
355.00	4.13	0.00	3.24	8.98	13.09	6.52
358.75	4.12	0.00	4.03	8.76	12.92	5.55
362.50	4.11	0.00	4.83	8.43	12.64	4.74
366.25	4.11	0.00	5.62	7.91	12.31	4.09
370.00	4.10	0.00	6.30	7.16	11.96	3.56
373.75	4.09	0.00	6.73	6.25	11.63	3.13
377.50	4.08	0.00	6.89	5.31	11.30	2.78
381.25	4.07	0.00	6.82	4.46	11.00	2.50
385.00	4.06	0.00	6.60	3.74	10.73	2.25
388.75	4.06	0.00	6.31	3.15	10.47	2.05
392.50	4.05	0.00	5.97	2.69	10.23	1.88
396.25	4.04	0.00	5.64	2.31	10.01	1.73
400.00	4.03	0.00	5.30	2.01	9.81	1.60

403.75	4.03	0.00	4.98	1.78	9.63	1.49
407.50	4.02	0.00	4.68	1.58	9.45	1.39
411.25	4.01	0.00	4.39	1.43	9.29	1.31
415.00	4.01	0.00	4.12	1.30	9.14	1.23
418.75	4.00	0.00	3.87	1.20	9.00	1.16
422.50	4.00	0.00	3.63	1.12	8.87	1.10
426.25	3.99	0.00	3.41	1.05	8.75	1.05
430.00	3.98	0.00	3.19	1.00	8.63	1.00
433.75	3.98	0.00	2.99	0.95	8.53	0.95
437.50	3.97	0.00	2.80	0.91	8.42	0.91
441.25	3.97	0.00	2.62	0.88	8.33	0.87
445.00	3.96	0.00	2.44	0.85	8.24	0.84
448.75	3.96	0.00	2.28	0.83	8.15	0.81
452.50	3.95	0.00	2.12	0.82	8.07	0.78
456.25	3.95	0.00	1.96	0.80	7.99	0.75
460.00	3.94	0.00	1.81	0.79	7.92	0.72
463.75	3.94	0.00	1.66	0.78	7.84	0.70
467.50	3.93	0.00	1.52	0.78	7.78	0.68
471.25	3.93	0.00	1.38	0.77	7.71	0.66
475.00	3.93	0.00	1.24	0.77	7.65	0.64
478.75	3.92	0.00	1.11	0.77	7.59	0.62
482.50	3.92	0.00	0.98	0.77	7.54	0.60
486.25	3.91	0.00	0.85	0.77	7.48	0.59
490.00	3.91	0.00	0.73	0.77	7.43	0.57
493.75	3.91	0.00	0.60	0.77	7.38	0.56
497.50	3.90	0.00	0.48	0.78	7.33	0.55
501.25	3.90	0.00	0.36	0.79	7.28	0.54
505.00	3.90	0.00	0.24	0.79	7.24	0.53
508.75	3.89	0.00	0.12	0.80	7.20	0.51
512.50	3.89	0.00	0.00	0.81	7.15	0.50
516.25	3.89	0.00	-0.12	0.82	7.11	0.49
520.00	3.88	0.00	-0.23	0.82	7.07	0.49
523.75	3.88	0.00	-0.34	0.83	7.04	0.48
527.50	3.88	0.00	-0.46	0.85	7.00	0.47
531.25	3.87	0.00	-0.57	0.86	6.96	0.46
535.00	3.87	0.00	-0.68	0.87	6.93	0.45
538.75	3.87	0.00	-0.80	0.88	6.90	0.45
542.50	3.87	0.00	-0.91	0.89	6.86	0.44
546.25	3.86	0.00	-1.02	0.91	6.83	0.44
550.00	3.86	0.00	-1.13	0.92	6.80	0.43
553.75	3.86	0.00	-1.24	0.93	6.77	0.42
557.50	3.85	0.00	-1.35	0.95	6.74	0.42
561.25	3.85	0.00	-1.46	0.96	6.71	0.41
565.00	3.85	0.00	-1.57	0.97	6.69	0.41
568.75	3.85	0.00	-1.68	0.99	6.66	0.41
572.50	3.85	0.00	-1.78	1.00	6.63	0.40

576.25	3.84	0.00	-1.89	1.02	6.61	0.40
580.00	3.84	0.00	-2.00	1.04	6.58	0.39
583.75	3.84	0.00	-2.11	1.05	6.56	0.39
587.50	3.84	0.00	-2.22	1.07	6.53	0.39
591.25	3.83	0.00	-2.33	1.08	6.51	0.39
595.00	3.83	0.00	-2.44	1.10	6.48	0.38
598.75	3.83	0.00	-2.55	1.12	6.46	0.38
602.50	3.83	0.00	-2.66	1.14	6.44	0.38
606.25	3.83	0.00	-2.77	1.15	6.42	0.38
610.00	3.82	0.00	-2.88	1.17	6.40	0.37
613.75	3.82	0.00	-2.99	1.19	6.37	0.37
617.50	3.82	0.00	-3.10	1.21	6.35	0.37
621.25	3.82	0.00	-3.21	1.23	6.33	0.37
625.00	3.82	0.00	-3.32	1.25	6.31	0.37
628.75	3.81	0.00	-3.43	1.27	6.29	0.37
632.50	3.81	0.00	-3.54	1.29	6.27	0.37
636.25	3.81	0.00	-3.65	1.31	6.26	0.37
640.00	3.81	0.00	-3.76	1.33	6.24	0.37
643.75	3.81	0.00	-3.87	1.35	6.22	0.37
647.50	3.81	0.00	-3.98	1.37	6.20	0.37
651.25	3.81	0.00	-4.10	1.39	6.18	0.37
655.00	3.80	0.00	-4.21	1.41	6.16	0.37
658.75	3.80	0.00	-4.32	1.43	6.15	0.37
662.50	3.80	0.00	-4.43	1.46	6.13	0.37
666.25	3.80	0.00	-4.55	1.48	6.11	0.37
670.00	3.80	0.00	-4.66	1.50	6.10	0.37
673.75	3.80	0.00	-4.78	1.53	6.08	0.37
677.50	3.79	0.00	-4.89	1.55	6.06	0.37
681.25	3.79	0.00	-5.00	1.57	6.05	0.37
685.00	3.79	0.00	-5.12	1.60	6.03	0.37
688.75	3.79	0.00	-5.24	1.62	6.01	0.37
692.50	3.79	0.00	-5.35	1.64	6.00	0.38
696.25	3.79	0.00	-5.47	1.67	5.98	0.38
700.00	3.79	0.00	-5.58	1.69	5.97	0.38
703.75	3.79	0.00	-5.70	1.72	5.95	0.38
707.50	3.78	0.00	-5.82	1.75	5.94	0.38
711.25	3.78	0.00	-5.94	1.77	5.92	0.39
715.00	3.78	0.00	-6.05	1.80	5.91	0.39
718.75	3.78	0.00	-6.17	1.82	5.89	0.39
722.50	3.78	0.00	-6.29	1.85	5.88	0.39
726.25	3.78	0.00	-6.41	1.88	5.86	0.40
730.00	3.78	0.00	-6.53	1.90	5.85	0.40
733.75	3.78	0.00	-6.65	1.93	5.83	0.40
737.50	3.78	0.00	-6.77	1.96	5.82	0.41
741.25	3.77	0.00	-6.89	1.99	5.81	0.41
745.00	3.77	0.00	-7.01	2.02	5.79	0.41

748.75	3.77	0.00	-7.14	2.05	5.78	0.42
752.50	3.77	0.00	-7.26	2.08	5.76	0.42
756.25	3.77	0.00	-7.38	2.10	5.75	0.43
760.00	3.77	0.00	-7.50	2.13	5.74	0.43
763.75	3.77	0.00	-7.63	2.16	5.72	0.44
767.50	3.77	0.00	-7.75	2.19	5.71	0.44
771.25	3.77	0.00	-7.88	2.22	5.70	0.45
775.00	3.77	0.00	-8.00	2.26	5.68	0.45
778.75	3.76	0.00	-8.13	2.29	5.67	0.46
782.50	3.76	0.00	-8.25	2.32	5.66	0.46
786.25	3.76	0.00	-8.38	2.35	5.64	0.47
790.00	3.76	0.00	-8.50	2.38	5.63	0.47
793.75	3.76	0.00	-8.63	2.41	5.62	0.48
797.50	3.76	0.00	-8.76	2.45	5.60	0.49
801.25	3.76	0.00	-8.89	2.48	5.59	0.49
805.00	3.76	0.00	-9.01	2.51	5.58	0.50
808.75	3.76	0.00	-9.14	2.55	5.56	0.51
812.50	3.76	0.00	-9.27	2.58	5.55	0.51
816.25	3.76	0.00	-9.40	2.62	5.54	0.52
820.00	3.75	0.00	-9.53	2.65	5.53	0.53
823.75	3.75	0.00	-9.66	2.68	5.51	0.54
827.50	3.75	0.00	-9.79	2.72	5.50	0.54
831.25	3.75	0.00	-9.92	2.76	5.49	0.55
835.00	3.75	0.00	-10.06	2.79	5.48	0.56
838.75	3.75	0.00	-10.19	2.83	5.47	0.57
842.50	3.75	0.00	-10.32	2.86	5.45	0.58
846.25	3.75	0.00	-10.45	2.90	5.44	0.59
850.00	3.75	0.00	-10.59	2.94	5.43	0.60
853.75	3.75	0.00	-10.72	2.98	5.42	0.61
857.50	3.75	0.00	-10.86	3.01	5.41	0.62
861.25	3.75	0.00	-10.99	3.05	5.39	0.63
865.00	3.75	0.00	-11.13	3.09	5.38	0.64
868.75	3.75	0.00	-11.26	3.13	5.37	0.65
872.50	3.74	0.00	-11.40	3.17	5.36	0.66
876.25	3.74	0.00	-11.53	3.21	5.35	0.68
880.00	3.74	0.00	-11.67	3.25	5.34	0.69
883.75	3.74	0.00	-11.81	3.29	5.33	0.70
887.50	3.74	0.00	-11.95	3.33	5.32	0.71
891.25	3.74	0.00	-12.09	3.37	5.31	0.73
895.00	3.74	0.00	-12.22	3.41	5.29	0.74
898.75	3.74	0.00	-12.36	3.45	5.28	0.75
902.50	3.74	0.00	-12.50	3.49	5.27	0.77
906.25	3.74	0.00	-12.64	3.53	5.26	0.78
910.00	3.74	0.00	-12.78	3.58	5.25	0.80
913.75	3.74	0.00	-12.93	3.62	5.25	0.81
917.50	3.74	0.00	-13.07	3.66	5.24	0.83

921.25	3.74	0.00	-13.21	3.70	5.23	0.84
925.00	3.74	0.00	-13.35	3.75	5.22	0.86
928.75	3.74	0.00	-13.49	3.79	5.21	0.87
932.50	3.74	0.00	-13.64	3.84	5.20	0.89
936.25	3.73	0.00	-13.78	3.88	5.19	0.91
940.00	3.73	0.00	-13.93	3.93	5.19	0.93
943.75	3.73	0.00	-14.07	3.97	5.18	0.94
947.50	3.73	0.00	-14.22	4.02	5.17	0.96
951.25	3.73	0.00	-14.36	4.06	5.16	0.98
955.00	3.73	0.00	-14.51	4.11	5.16	1.00
958.75	3.73	0.00	-14.65	4.16	5.15	1.02
962.50	3.73	0.00	-14.80	4.20	5.15	1.04
966.25	3.73	0.00	-14.95	4.25	5.14	1.06
970.00	3.73	0.00	-15.10	4.30	5.13	1.08
973.75	3.73	0.00	-15.24	4.35	5.13	1.10
977.50	3.73	0.00	-15.39	4.40	5.13	1.12
981.25	3.73	0.00	-15.54	4.44	5.12	1.14
985.00	3.73	0.00	-15.69	4.49	5.12	1.17
988.75	3.73	0.00	-15.84	4.54	5.12	1.19
992.50	3.73	0.00	-15.99	4.59	5.11	1.21
996.25	3.73	0.00	-16.14	4.64	5.11	1.23
1000.00	3.73	0.00	-16.29	4.69	5.11	1.26

Table S2**.** Tabulated optical constants of vdW $MoOCl_2$.

λ (nm)	n_z	k_z	n_x	k_x	n_y	k_y
250.00	2.22	0.00	0.96	1.14	1.98	1.11
253.75	2.21	0.00	0.97	1.18	2.04	1.15
257.50	2.20	0.00	0.97	1.22	2.07	1.14
261.25	2.20	0.00	0.98	1.26	2.08	1.12
265.00	2.19	0.00	0.99	1.31	2.05	1.09
268.75	2.19	0.00	1.00	1.36	2.00	1.09
272.50	2.18	0.00	1.01	1.41	1.92	1.11
276.25	2.18	0.00	1.02	1.46	1.84	1.16
280.00	2.17	0.00	1.04	1.51	1.76	1.26
283.75	2.17	0.00	1.06	1.56	1.71	1.40
287.50	2.16	0.00	1.09	1.62	1.69	1.57
291.25	2.16	0.00	1.12	1.67	1.73	1.74
295.00	2.16	0.00	1.16	1.73	1.82	1.91
298.75	2.15	0.00	1.20	1.78	1.94	2.05
302.50	2.15	0.00	1.25	1.84	2.08	2.17
306.25	2.15	0.00	1.31	1.89	2.22	2.28
310.00	2.14	0.00	1.36	1.94	2.40	2.40
313.75	2.14	0.00	1.43	1.99	2.63	2.51
317.50	2.14	0.00	1.50	2.03	2.95	2.55

321.25	2.13	0.00	1.57	2.08	3.29	2.46
325.00	2.13	0.00	1.65	2.13	3.55	2.25
328.75	2.13	0.00	1.75	2.17	3.70	2.02
332.50	2.12	0.00	1.87	2.22	3.78	1.83
336.25	2.12	0.00	2.01	2.25	3.85	1.67
340.00	2.12	0.00	2.17	2.25	3.92	1.50
343.75	2.12	0.00	2.35	2.21	3.97	1.30
347.50	2.11	0.00	2.51	2.13	3.97	1.11
351.25	2.11	0.00	2.65	2.01	3.93	0.94
355.00	2.11	0.00	2.75	1.88	3.87	0.80
358.75	2.11	0.00	2.84	1.75	3.79	0.68
362.50	2.10	0.00	2.92	1.61	3.72	0.59
366.25	2.10	0.00	2.98	1.44	3.65	0.52
370.00	2.10	0.00	3.00	1.26	3.59	0.46
373.75	2.10	0.00	2.98	1.08	3.52	0.41
377.50	2.10	0.00	2.92	0.92	3.47	0.37
381.25	2.09	0.00	2.85	0.79	3.42	0.34
385.00	2.09	0.00	2.76	0.68	3.37	0.31
388.75	2.09	0.00	2.67	0.59	3.33	0.29
392.50	2.09	0.00	2.58	0.53	3.28	0.27
396.25	2.09	0.00	2.49	0.47	3.25	0.25
400.00	2.09	0.00	2.41	0.43	3.21	0.23
403.75	2.08	0.00	2.33	0.39	3.18	0.22
407.50	2.08	0.00	2.25	0.36	3.15	0.21
411.25	2.08	0.00	2.18	0.34	3.12	0.20
415.00	2.08	0.00	2.11	0.32	3.10	0.19
418.75	2.08	0.00	2.04	0.31	3.07	0.18
422.50	2.08	0.00	1.98	0.30	3.05	0.17
426.25	2.08	0.00	1.91	0.29	3.03	0.16
430.00	2.08	0.00	1.85	0.28	3.01	0.16
433.75	2.07	0.00	1.79	0.28	2.99	0.15
437.50	2.07	0.00	1.73	0.28	2.97	0.15
441.25	2.07	0.00	1.67	0.28	2.95	0.14
445.00	2.07	0.00	1.61	0.28	2.94	0.14
448.75	2.07	0.00	1.56	0.28	2.92	0.13
452.50	2.07	0.00	1.50	0.29	2.90	0.13
456.25	2.07	0.00	1.44	0.30	2.89	0.12
460.00	2.07	0.00	1.39	0.30	2.88	0.12
463.75	2.07	0.00	1.33	0.31	2.86	0.12
467.50	2.06	0.00	1.27	0.32	2.85	0.11
471.25	2.06	0.00	1.22	0.34	2.84	0.11
475.00	2.06	0.00	1.16	0.35	2.83	0.11
478.75	2.06	0.00	1.10	0.37	2.82	0.11
482.50	2.06	0.00	1.04	0.39	2.80	0.10
486.25	2.06	0.00	0.98	0.42	2.79	0.10
490.00	2.06	0.00	0.92	0.44	2.78	0.10

493.75	2.06	0.00	0.87	0.47	2.78	0.10
497.50	2.06	0.00	0.81	0.51	2.77	0.09
501.25	2.06	0.00	0.75	0.55	2.76	0.09
505.00	2.06	0.00	0.70	0.60	2.75	0.09
508.75	2.05	0.00	0.65	0.65	2.74	0.09
512.50	2.05	0.00	0.61	0.70	2.73	0.09
516.25	2.05	0.00	0.57	0.76	2.72	0.09
520.00	2.05	0.00	0.53	0.81	2.72	0.09
523.75	2.05	0.00	0.51	0.87	2.71	0.08
531.25	2.05	0.00	0.46	0.98	2.69	0.08
535.00	2.05	0.00	0.44	1.03	2.69	0.08
538.75	2.05	0.00	0.43	1.08	2.68	0.08
542.50	2.05	0.00	0.41	1.13	2.67	0.08
546.25	2.05	0.00	0.40	1.18	2.67	0.08
550.00	2.05	0.00	0.39	1.22	2.66	0.08
553.75	2.05	0.00	0.38	1.27	2.66	0.08
557.50	2.05	0.00	0.37	1.31	2.65	0.08
561.25	2.05	0.00	0.37	1.35	2.64	0.07
565.00	2.04	0.00	0.36	1.40	2.64	0.07
568.75	2.04	0.00	0.35	1.44	2.63	0.07
572.50	2.04	0.00	0.35	1.47	2.63	0.07
576.25	2.04	0.00	0.35	1.51	2.62	0.07
580.00	2.04	0.00	0.34	1.55	2.62	0.07
583.75	2.04	0.00	0.34	1.59	2.61	0.07
587.50	2.04	0.00	0.34	1.62	2.61	0.07
591.25	2.04	0.00	0.33	1.66	2.60	0.07
595.00	2.04	0.00	0.33	1.69	2.60	0.07
598.75	2.04	0.00	0.33	1.73	2.59	0.07
602.50	2.04	0.00	0.33	1.76	2.59	0.07
606.25	2.04	0.00	0.33	1.79	2.58	0.07
610.00	2.04	0.00	0.32	1.83	2.58	0.07
613.75	2.04	0.00	0.32	1.86	2.58	0.07
617.50	2.04	0.00	0.32	1.89	2.57	0.07
621.25	2.04	0.00	0.32	1.92	2.57	0.07
625.00	2.04	0.00	0.32	1.95	2.56	0.07
628.75	2.04	0.00	0.32	1.98	2.56	0.07
632.50	2.04	0.00	0.32	2.01	2.55	0.07
636.25	2.04	0.00	0.32	2.04	2.55	0.07
640.00	2.04	0.00	0.32	2.07	2.55	0.07
643.75	2.04	0.00	0.32	2.10	2.54	0.07
647.50	2.03	0.00	0.32	2.13	2.54	0.07
651.25	2.03	0.00	0.32	2.16	2.54	0.07
655.00	2.03	0.00	0.32	2.18	2.53	0.07
658.75	2.03	0.00	0.32	2.21	2.53	0.07
662.50	2.03	0.00	0.32	2.24	2.52	0.07
666.25	2.03	0.00	0.32	2.26	2.52	0.07

670.00	2.03	0.00	0.32	2.29	2.52	0.07
673.75	2.03	0.00	0.32	2.32	2.51	0.07
677.50	2.03	0.00	0.33	2.34	2.51	0.07
681.25	2.03	0.00	0.33	2.37	2.51	0.07
685.00	2.03	0.00	0.33	2.40	2.50	0.07
688.75	2.03	0.00	0.33	2.42	2.50	0.07
692.50	2.03	0.00	0.33	2.45	2.50	0.07
696.25	2.03	0.00	0.33	2.47	2.49	0.07
700.00	2.03	0.00	0.33	2.50	2.49	0.07
703.75	2.03	0.00	0.33	2.52	2.49	0.07
707.50	2.03	0.00	0.33	2.55	2.48	0.07
711.25	2.03	0.00	0.34	2.57	2.48	0.07
715.00	2.03	0.00	0.34	2.60	2.48	0.07
718.75	2.03	0.00	0.34	2.62	2.47	0.07
722.50	2.03	0.00	0.34	2.65	2.47	0.07
726.25	2.03	0.00	0.34	2.67	2.47	0.07
730.00	2.03	0.00	0.34	2.69	2.47	0.08
733.75	2.03	0.00	0.34	2.72	2.46	0.08
737.50	2.03	0.00	0.34	2.74	2.46	0.08
741.25	2.03	0.00	0.35	2.77	2.46	0.08
745.00	2.03	0.00	0.35	2.79	2.45	0.08
748.75	2.03	0.00	0.35	2.81	2.45	0.08
752.50	2.03	0.00	0.35	2.84	2.45	0.08
756.25	2.03	0.00	0.35	2.86	2.44	0.08
760.00	2.03	0.00	0.35	2.88	2.44	0.08
763.75	2.03	0.00	0.36	2.90	2.44	0.08
767.50	2.03	0.00	0.36	2.93	2.44	0.08
771.25	2.03	0.00	0.36	2.95	2.43	0.08
775.00	2.03	0.00	0.36	2.97	2.43	0.09
778.75	2.02	0.00	0.36	2.99	2.43	0.09
782.50	2.02	0.00	0.36	3.02	2.42	0.09
786.25	2.02	0.00	0.37	3.04	2.42	0.09
790.00	2.02	0.00	0.37	3.06	2.42	0.09
793.75	2.02	0.00	0.37	3.08	2.42	0.09
797.50	2.02	0.00	0.37	3.11	2.41	0.09
801.25	2.02	0.00	0.37	3.13	2.41	0.09
805.00	2.02	0.00	0.38	3.15	2.41	0.10
808.75	2.02	0.00	0.38	3.17	2.40	0.10
812.50	2.02	0.00	0.38	3.19	2.40	0.10
816.25	2.02	0.00	0.38	3.21	2.40	0.10
820.00	2.02	0.00	0.38	3.24	2.40	0.10
823.75	2.02	0.00	0.39	3.26	2.39	0.10
827.50	2.02	0.00	0.39	3.28	2.39	0.10
831.25	2.02	0.00	0.39	3.30	2.39	0.11
835.00	2.02	0.00	0.39	3.32	2.38	0.11
838.75	2.02	0.00	0.39	3.34	2.38	0.11

842.50	2.02	0.00	0.40	3.36	2.38	0.11
846.25	2.02	0.00	0.40	3.38	2.38	0.11
850.00	2.02	0.00	0.40	3.41	2.37	0.12
853.75	2.02	0.00	0.40	3.43	2.37	0.12
857.50	2.02	0.00	0.40	3.45	2.37	0.12
861.25	2.02	0.00	0.41	3.47	2.37	0.12
865.00	2.02	0.00	0.41	3.49	2.36	0.12
868.75	2.02	0.00	0.41	3.51	2.36	0.13
872.50	2.02	0.00	0.41	3.53	2.36	0.13
876.25	2.02	0.00	0.41	3.55	2.36	0.13
880.00	2.02	0.00	0.42	3.57	2.35	0.13
881.88	2.02	0.00	0.42	3.58	2.35	0.14
883.75	2.02	0.00	0.42	3.59	2.35	0.14
887.50	2.02	0.00	0.42	3.61	2.35	0.14
891.25	2.02	0.00	0.42	3.63	2.35	0.14
895.00	2.02	0.00	0.42	3.65	2.34	0.14
898.75	2.02	0.00	0.43	3.67	2.34	0.15
902.50	2.02	0.00	0.43	3.69	2.34	0.15
906.25	2.02	0.00	0.43	3.71	2.34	0.15
910.00	2.02	0.00	0.43	3.73	2.33	0.16
913.75	2.02	0.00	0.44	3.75	2.33	0.16
917.50	2.02	0.00	0.44	3.77	2.33	0.16
921.25	2.02	0.00	0.44	3.79	2.33	0.17
925.00	2.02	0.00	0.44	3.81	2.32	0.17
928.75	2.02	0.00	0.45	3.83	2.32	0.17
932.50	2.02	0.00	0.45	3.85	2.32	0.18
936.25	2.02	0.00	0.45	3.87	2.32	0.18
940.00	2.02	0.00	0.45	3.89	2.32	0.19
943.75	2.02	0.00	0.45	3.91	2.31	0.19
947.50	2.02	0.00	0.46	3.93	2.31	0.19
951.25	2.02	0.00	0.46	3.95	2.31	0.20
955.00	2.02	0.00	0.46	3.97	2.31	0.20
958.75	2.02	0.00	0.46	3.99	2.31	0.21
962.50	2.02	0.00	0.47	4.01	2.30	0.21
966.25	2.02	0.00	0.47	4.03	2.30	0.21
970.00	2.02	0.00	0.47	4.05	2.30	0.22
973.75	2.02	0.00	0.47	4.07	2.30	0.22
977.50	2.02	0.00	0.48	4.09	2.30	0.23
981.25	2.02	0.00	0.48	4.11	2.30	0.23
985.00	2.02	0.00	0.48	4.13	2.30	0.24
988.75	2.02	0.00	0.48	4.14	2.30	0.24
992.50	2.02	0.00	0.48	4.16	2.30	0.25
996.25	2.02	0.00	0.49	4.18	2.29	0.25
1000.00	2.02	0.00	0.49	4.20	2.29	0.26

Supplementary Note 5: Differential reflectance contrast maps (an extended dataset)

Additional micro-reflectance spectroscopy data for vdW $MoOCl_2$ samples are presented below.

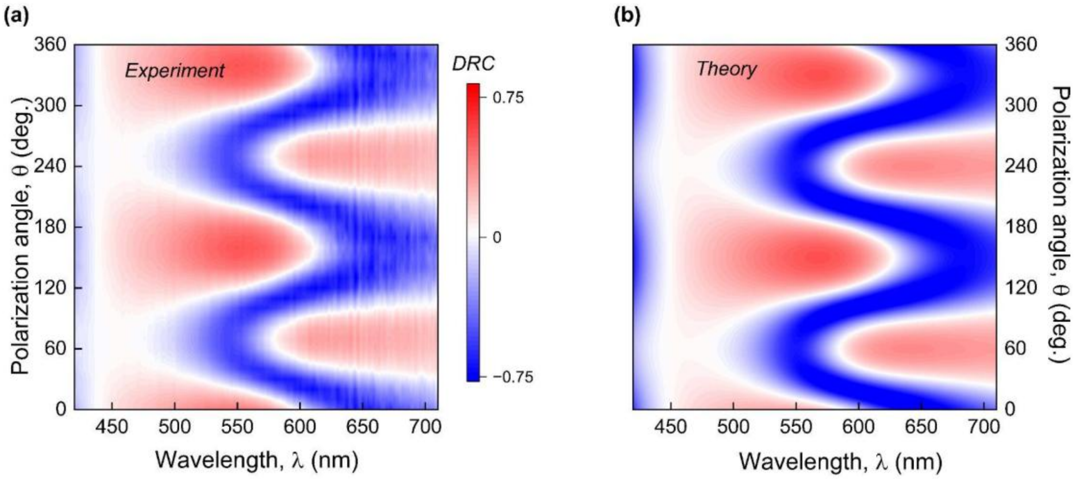

Fig. S10| **a)** Experimental angle-resolved DRC map of a representative 15 nm-thick vdW $MoOCl_2$ sample exfoliated onto a 295 nm Si/SiO_2 substrate. **b)** Theoretical angle-resolved DRC map calculated using the optical constants extracted from (a).

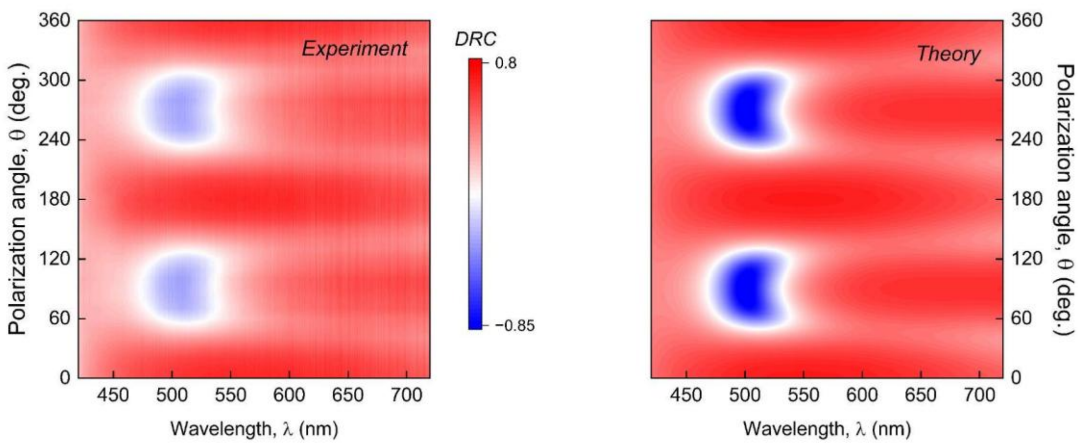

Fig. S11|**a)** Experimental angle-resolved DRC map of a representative 50 nm-thick vdW $MoOCl_2$ sample exfoliated onto a 90 nm Si/SiO_2 substrate. **b)** Theoretical angle-resolved DRC map calculated using the optical constants extracted from (a).

Supplementary Note 6: Simulated axis dependent reflectance spectra of vdW $MoOCl_2$ (an extended dataset)

Additional simulated reflectance spectra of vdW $MoOCl_2$ samples with different thicknesses are shown for incident polarization sequentially aligned with the *x* and *y* axes.

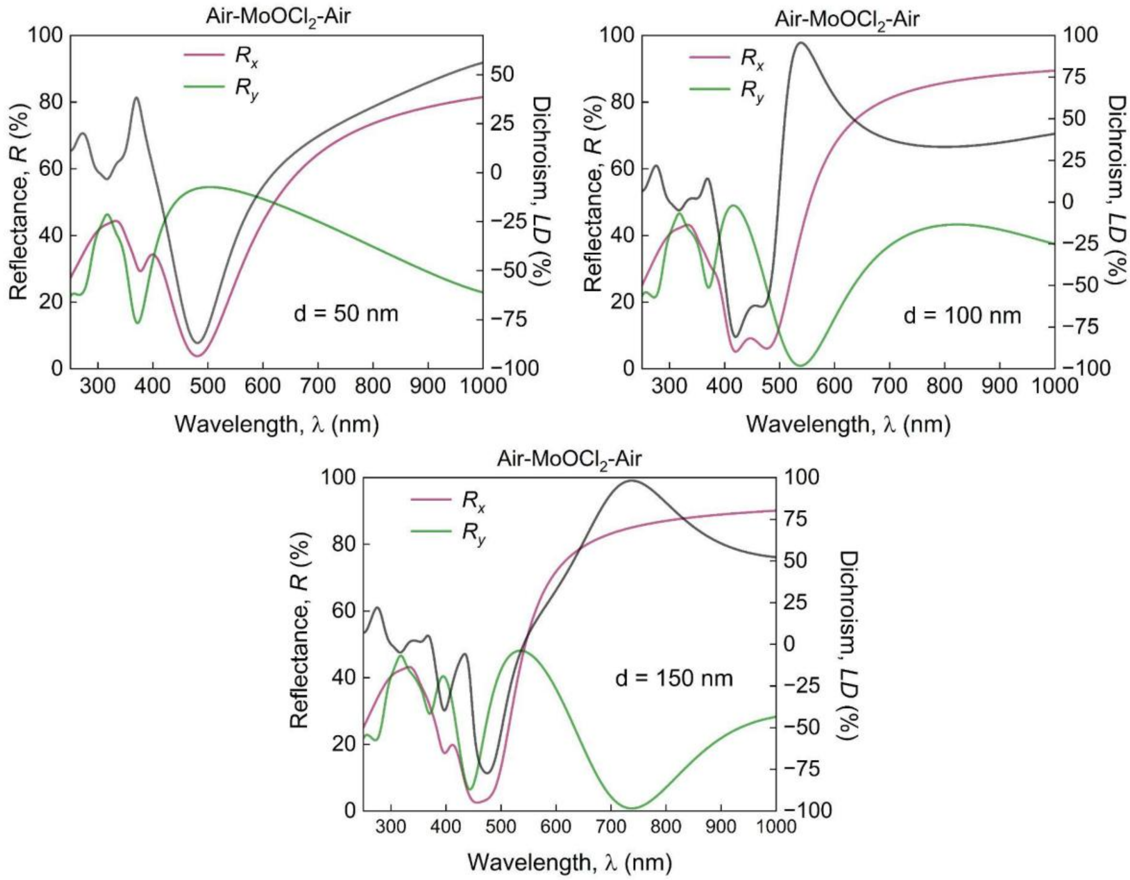

Fig. S12|Simulated reflectance spectra of 50, 100, and 150 nm-thick vdW $MoOCl_2$ samples for incident polarization aligned sequentially with the *x* and *y* axes. The black curve represents the linear dichroism (LD) in reflectance between the metallic *x* and insulating *y* axes.

We employed the transfer-matrix method [1] to calculate the differential reflectance contrast. The multilayer optical stack used in these calculations consisted of vdW $MoOCl_2$ samples of varying thickness exfoliated onto a SiO_2/Si substrate (Air/$MoOCl_2$/SiO_2/Si configuration). Electromagnetic propagation through the stack was modeled by applying the standard boundary conditions at each interface. Because vdW $MoOCl_2$ is biaxially anisotropic, the boundary conditions were written separately for the two orthogonal in-plane principal axes, $j = \{x, y\}$. At normal incidence, the Air → vdW $MoOCl_2$ boundary-condition matrix for $j -$ axis is

$$B_{air-SiP_j} = \begin{bmatrix} \frac{n_{air}}{n_j}+1 & 0 & \frac{n_{air}}{n_j}-1 & 0 \\ 0 & \frac{n_{air}}{n_j}+1 & 0 & \frac{n_{air}}{n_j}-1 \\ \frac{n_{air}}{n_j}-1 & 0 & \frac{n_{air}}{n_j}+1 & 0 \\ 0 & \frac{n_{air}}{n_j}-1 & 0 & \frac{n_{air}}{n_j}+1 \end{bmatrix}, \quad (5.1)$$

and analogous matrices apply to the vdW $MoOCl_2$ → SiO_2 and SiO_2 → Si interfaces, where n_j is the in-plane refractive index of the $MoOCl_2$ along the j −axis.

The propagation matrix for the biaxial vdW $MoOCl_2$ layer can be written as:

$$P_{MoOCl2} = \begin{bmatrix} e^{ik_jd} & 0 & 0 & 0 \\ 0 & e^{ik_jd} & 0 & 0 \\ 0 & 0 & e^{-ik_jd} & 0 \\ 0 & 0 & 0 & e^{-ik_jd} \end{bmatrix}, \quad (5.2)$$

where $k_j = \frac{2\pi}{\lambda} n_j$ and *d* is vdW $MoOCl_2$-layer thickness.

With the layer thicknesses set and the boundary and propagation matrices assembled, the total transfer matrix for each in-plane axis becomes:

$$M_j = B_{air-MoOCl2_j} \times P_{MoOCl2_j} \times B_{MoOCl2_j-\mathrm{SiO_2}} \times P_{\mathrm{SiO_2}} \times B_{\mathrm{SiO_2-Si}}, \qquad j = x, y. \quad (5.3)$$

The corresponding reflection amplitudes are obtained from the matrix elements:

$$r_j = \frac{M_{j_{3,1}}}{M_{j_{1,1}}}. \quad (5.4)$$

The polarization-resolved reflectance is obtained by accounting for the relative orientations of the polarizer and analyzer. The total reflection coefficient is therefore

$$r = r_x \cos(\phi - \theta)\cos(\theta) - r_y \sin(\phi - \theta)\sin(\theta), \quad (5.5)$$

where ϕ is the angle between the polarizer and analyzer, and θ is the angle between the analyzer and the principal optical axis of vdW $MoOCl_2$ sample.

Note that, to obtain the differential reflectance, the reflection coefficient of the reference Air/SiO_2/Si stack (r_{ref}) is also calculated and its reflectance is then subtracted from that of the full stack. The differential-reflectance contrast is defined as

$$R_{DRC} = \frac{R - R_{ref}}{R + \mathrm{R}_{ref}}, \quad (5.6)$$

where $R_{ref} = |r_{ref}|^2$ and $R = |r|^2$ are the reflectances of the reference and full system, respectively.

Supplementary Note 7: Calculations of chirality and circular dichroism for twisted bilayer vdW $MoOCl_2$

The transmittance and reflectance spectra of vdW $MoOCl_2$ heterostructure were calculated using generalized transfer-matrix method [1]. In this method, the propagation matrix (7.1) and the boundary-condition matrices (7.2) are defined as follows:

$$P_i = \begin{bmatrix} e^{-i\frac{2\pi}{\lambda}q_{i1}d_i} & 0 & 0 & 0 \\ 0 & e^{-i\frac{2\pi}{\lambda}q_{i2}d_i} & 0 & 0 \\ 0 & 0 & e^{-i\frac{2\pi}{\lambda}q_{i3}d_i} & 0 \\ 0 & 0 & 0 & e^{-i\frac{2\pi}{\lambda}q_{i4}d_i} \end{bmatrix}, \quad (7.1)$$

$$A_i = \begin{bmatrix} \gamma_{i11} & \gamma_{i21} & \gamma_{i31} & \gamma_{i41} \\ \gamma_{i12} & \gamma_{i22} & \gamma_{i32} & \gamma_{i42} \\ \frac{q_{i1}\gamma_{i11}-\xi\gamma_{i13}}{\mu_i} & \frac{q_{i2}\gamma_{i21}-\xi\gamma_{i23}}{\mu_i} & \frac{q_{i3}\gamma_{i31}-\xi\gamma_{i33}}{\mu_i} & \frac{q_{i4}\gamma_{i41}-\xi\gamma_{i43}}{\mu_i} \\ \frac{1}{\mu_i}q_{i1}\gamma_{i12} & \frac{1}{\mu_i}q_{i2}\gamma_{i22} & \frac{1}{\mu_i}q_{i3}\gamma_{i32} & \frac{1}{\mu_i}q_{i4}\gamma_{i42} \end{bmatrix}, \quad (7.2)$$

where the quantities qij represent the eigenvalues of the Maxwell eigenproblem for layer i,corresponding to the z-components of the wave-vector for the four eigenmodes of the material. The associated eigenvector components γ_{ijk} are obtained from the 4×3 eigenmode matrix; and because the materials are non-magnetic and the incidence is normal ($\theta = 0$), we set the permeability $\mu = 1$, and the in-plane wave-vector component $\xi = 0$.

After defining the constituent matrices, the total transfer matrix (7.3) of the system is constructed, accounting for the boundary conditions at both the superstrate and substrate.

$$T_{tot} = A_{sup}^{-1} \prod_{i=1}^{N} A_i P_i A_i^{-1} A_{sub}, \quad (7.3)$$

where, A_{sup} and A_{sub} represent the boundary conditions at the substrate and superstrate, respectively. After constructing the total transfer matrix, we apply the normalization $T \rightarrow \Gamma^*$and then evaluate the polarization-dependent transmittance coefficients (7.4).

$$t_{pp} = \frac{\Gamma_{33}^*}{\Gamma_{11}^*\Gamma_{33}^* - \Gamma_{13}^*\Gamma_{31}^*}; \qquad t_{ps} = \frac{-\Gamma_{31}^*}{\Gamma_{11}^*\Gamma_{33}^* - \Gamma_{13}^*\Gamma_{31}^*}; \quad (7.4)$$

$$t_{ss} = \frac{\Gamma_{11}^*}{\Gamma_{11}^*\Gamma_{33}^* - \Gamma_{13}^*\Gamma_{31}^*}; \qquad t_{sp} = \frac{-\Gamma_{13}^*}{\Gamma_{11}^*\Gamma_{33}^* - \Gamma_{13}^*\Gamma_{31}^*}.$$

The basis transformation into the RCP/LCP basis is performed by applying the circular-polarization Jones matrices M_{Circ} to the 2 × 2 transmission matrix.

$$M_{Circ} = \frac{1}{\sqrt{2}}\begin{bmatrix} 1 & 1 \\ i & -i \end{bmatrix},$$

$$t_{Circ} = M_{Circ}^{-1}\, t\, M_{Circ} = \begin{bmatrix} t_{RR} & t_{RL} \\ t_{LR} & t_{LL} \end{bmatrix}. \tag{7.5}$$

We then define the transmittances for right- and left-circularly polarized light as $T_{RCP} = |t_{RR}|^2$ and $T_{LCP} = |t_{LL}|^2$, respectively. The circular dichroism is then given by $CD = T_{RCP} - T_{LCP}$.

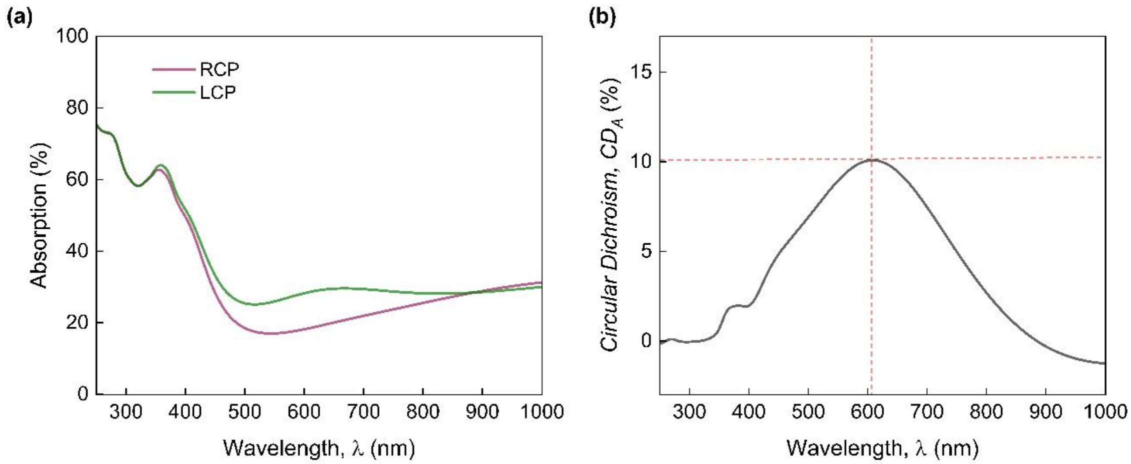

Fig. S13|**a)** Calculated absorption of RCP and LCP light, obtained as $A = 1 - R - T$, for light traversing the vdW heterostructure. **b)** Corresponding circular dichroism in absorption (CD_A) , defined as the difference between the RCP and LCP absorption shown in (a).

By calculating the transmission and reflection using the generalized transfer-matrix method described above, we also obtain the absorption of circularly polarized light as $A = 1 - R - T$. The corresponding absorption spectra for the vdW $MoOCl_2$ bilayer are presented in Fig. S12 together with the circular dichroism in absorption defined as the difference between the two circular channels, $CD_A = A_{RCP} - A_{LCP}$.

References

1. Passler, N. C. & Paarmann, A. Generalized 4 × 4 matrix formalism for light propagation in anisotropic stratified media: study of surface phonon polaritons in polar dielectric heterostructures. *J. Opt. Soc. Am. B* **34**, 2128–2139 (2017).